Circular Dichroism and Magnetic Circular Dichroism of *Azotobacter vinelandii* Ferredoxin I[†]

P. J. Stephens,[*,‡] G. M. Jensen,[‡] F. J. Devlin,[‡] T. V. Morgan,[§] C. D. Stout,[∥] A. E. Martin,[⊥] and B. K. Burgess[⊥]

Department of Chemistry, University of Southern California, Los Angeles, California 90089-0482, Department of Chemistry, University of Georgia, Athens, Georgia 30602, Department of Molecular Biology, Research Institute of Scripps Clinic, 10666 North Torrey Pines Road, LaJolla, California 92037, and Department of Molecular Biology and Biochemistry, University of California, Irvine, California 92717

Received May 14, 1990; Revised Manuscript Received November 19, 1990

ABSTRACT: Room temperature circular dichroism (CD) and low temperature magnetic circular dichroism (MCD) spectra of air-oxidized and dithionite-reduced *Azotobacter vinelandii* ferredoxin I (FdI), a {[4Fe-4S]$^{2+/1+}$, [3Fe-4S]$^{1+/0}$} protein, are reported. Unlike the CD of oxidized FdI, the CD of dithionite-reduced FdI exhibits significant pH dependence, consistent with protonation–deprotonation at or near the cluster reduced: the [3Fe-4S] cluster. The MCD of reduced FdI, which originates in the paramagnetic reduced [3Fe-4S]^0 cluster, is also pH-dependent. Detailed studies of the field dependence and temperature dependence of the MCD of oxidized and reduced FdI, in the latter case at pH 6.0 and 8.3, are reported. The low-field temperature dependence of the MCD of oxidized FdI, which originates in the paramagnetic oxidized [3Fe-4S]$^{1+}$ cluster, establishes the absence of a significant population of excited electronic states of this cluster up to 60 K. The low-field temperature dependence of the MCD of reduced FdI establishes that the ground-state manifold of the reduced [3Fe-4S]^0 cluster possesses $S \geq 2$ at both pH 6.0 and 8.3. Analysis, assuming $S = 2$ and an axial zero-field splitting Hamiltonian, leads to $D = -2.0$ and -3.5 cm^{-1} at pH 6.0 and 8.3, respectively. The site of the (de)protonation affecting the spectroscopic properties of the [3Fe-4S] cluster remains unknown.

Azotobacter vinelandii ferredoxin I (FdI) has a long and checkered history. Yoch et al. (1969) and Shethna (1970) first reported the purification of FdI. Yoch et al. (1969) demonstrated the reduction of FdI by sodium dithionite (DT) and the ability of FdI to convey electrons to *A. vinelandii* nitrogenase from illuminated chloroplasts, implicating FdI as a possible proximal reductant of nitrogenase. Extensive characterization of FdI was carried out by Yoch and Arnon (1972). Inter alia, Fe (~8), S^{2-} (~8), and amino acid analyses (including ~8 cysteines) and a midpoint potential of −420 mV (vs SHE) for the reduction of FdI were reported.

These initial studies thus appeared to place FdI in the category of low-potential bacterial ferredoxins typified by *Clostridium pasteurianum* ferredoxin (*Cp*Fd) and the crystallographically characterized *Peptococcus aerogenes* ferredoxin (Adman et al., 1976) and containing two [4Fe-4S]$^{2+/1+}$ clusters (Sweeney & Rabinowitz, 1980). Further studies by Sweeney et al. (1975) modified this conclusion, however. FdI was shown to exhibit nearly isotropic $g \sim 2.01$ EPR at liquid helium temperatures, vanishing on reduction (using illuminated chloroplasts) and increasing in intensity on addition of $Fe(CN)_6^{3-}$. Sweeney et al. (1975) concluded that FdI contains two HiPIP-like [4Fe-4S]$^{3+/2+}$ clusters (Sweeney & Rabinowitz, 1980), one possessing a high and the other a low midpoint potential. In subsequent electrochemical studies, Yoch and Carithers (1978) remeasured the midpoint potentials for oxidation and reduction, reporting +320 and −424 mV (vs SHE), respectively.

Further studies of FdI by X-ray crystallography (Stout et al., 1980; Ghosh et al., 1981; 1982), carried out in parallel with (and leading to a structure consistent with the results of) direct sequence determination (Howard et al., 1983), and by Mössbauer spectroscopy (Emptage et al., 1980) led to the conclusion that FdI contains one [4Fe-4S] cluster and one novel cluster containing 3 Fe. X-ray crystallography found a [4Fe-4S] cluster identical in stoichiometry, $Fe_4S_4(S\text{-}Cys)_4$, and essentially identical in structure with those in *P. aerogenes* ferredoxin (*Pa*Fd) (Adman et al., 1976) and *Chromatium vinosum* HiPIP (Freer et al., 1975). The 3Fe cluster was reported to have $Fe_3S_3(S\text{-}Cys)_5X$ (X being H_2O or OH^-) stoichiometry with a nearly planar Fe_3S_3 core. The cysteine content of FdI was thereby increased to 9. Mössbauer spectroscopy (Emptage et al., 1980) of air-oxidized FdI identified the 3Fe cluster with the $g \sim 2.01$ EPR and showed the [4Fe-4S] cluster to be in the EPR silent, 2+ oxidation state. Studies of DT-reduced FdI showed the 3Fe cluster to be reduced to an EPR silent paramagnetic state with $S \geq 1$ and the [4Fe-4S]$^{2+}$ cluster to be unaffected. Subsequent analysis (Kent et al., 1982) established an all-ferric oxidation level for the oxidized 3Fe cluster.

Subsequent studies of the $Fe(CN)_6^{3-}$ oxidation of FdI using UV–visible absorption, circular dichroism (CD), magnetic circular dichroism (MCD), and EPR spectroscopies showed that the [4Fe-4S] cluster of FdI does not in fact exhibit oxidation to the 3+ level, but instead can be reduced to the 1+ level, albeit at extremely low potentials (Morgan et al., 1984). The $Fe(CN)_6^{3-}$ oxidation of FdI was shown to be destructive in nature, proceeding initially at the [4Fe-4S] cluster and via an EPR active intermediate identified as a 3-electron oxidation product in which a cysteinyldisulfide radical is formed. Detailed MCD and EPR studies (Morgan et al., 1985) further characterized the $Fe(CN)_6^{3-}$ oxidation of FdI, showing that the destruction of the 3Fe cluster follows sequentially the

[†] This research was supported by the National Science Foundation and the National Institutes of Health.

* To whom correspondence should be addressed.
[‡] University of Southern California.
[§] University of Georgia.
[∥] Research Institute of Scripps Clinic.
[⊥] University of California.

0006-2960/91/0430-3200$02.50/0

destruction of the [4Fe-4S] cluster. It is therefore possible to obtain an oxidation product of FdI containing only the 3Fe cluster: (3Fe)FdI. The MCD and EPR of (3Fe)FdI showed (Stephens et al., 1985) that the 3Fe cluster of (3Fe)FdI is essentially identical with that of FdI. EXAFS studies (Stephens et al., 1985) of (3Fe)FdI found Fe–Fe distances of ~2.7 Å, very different from those (~4.1 Å) obtained by X-ray crystallography of FdI (Ghosh et al. 1981, 1982). It was concluded that either the X-ray or EXAFS studies were incorrect or the structure of the 3Fe cluster differs in solution and crystalline states.

Very recently, the X-ray structure of FdI has been redetermined (Stout et al., 1988; Stout, 1988, 1989). The 3Fe cluster has been shown to possess $Fe_3S_4(S\text{-}Cys)_3$ stoichiometry and a cubane-like Fe_3S_4 core with Fe–Fe distances of ~2.7 Å. Cysteines 8, 16, and 49 ligate the [3Fe-4S] cluster while cysteines 20, 39, 42, and 45 ligate the [4Fe-4S] cluster. The nonligating cysteines 11 and 24 lie near the [3Fe-4S] and [4Fe-4S] clusters, respectively, cysteine 24 being in van der Waals contact with an inorganic sulfide on the [4Fe-4S] cluster (Stout, 1988, 1989). The [3Fe-4S] cluster structure is essentially identical with that of [3Fe-4S] clusters in pig heart aconitase (Robbins & Stout, 1989a,b) and *Desulfovibrio gigas* ferredoxin II (*Dg*FdII) (Kissinger et al., 1988, 1989), both of which were also very recently characterized by X-ray crystallography.

While the structure of FdI in its as-isolated, air-oxidized $\{[4Fe\text{-}4S]^{2+}, [3Fe\text{-}4S]^{1+}\}$ state is now well-defined, a variety of interesting questions regarding the chemical and spectroscopic properties of FdI remain unresolved. Studies of the closely related *Azotobacter chroococcum* ferredoxin (*Ac*FdI) found evidence of a dramatic pH dependence of the MCD spectrum in the DT-reduced state (George et al., 1984). Since this is in turn attributable to the $[3Fe\text{-}4S]^0$ cluster, it was concluded that this cluster exists in acid and alkaline forms. The MCD of the alkaline form of the $[3Fe\text{-}4S]^0$ cluster closely resembles that previously reported for reduced $[3Fe\text{-}4S]^0$ clusters in other proteins. The MCD of the acid form of the $[3Fe\text{-}4S]^0$ cluster is extremely different and unique. The pK_a of this pH effect was estimated to be ~7.5. Subsequently, a pH dependence of the reduction potential of the [3Fe-4S] cluster of *Ac*FdI was observed and identified with the pH dependence of the $[3Fe\text{-}4S]^0$ MCD (Armstrong et al., 1988). MCD studies of FdI also confirmed the existence of an analogous phenomenon in the *A. vinelandii* protein (Johnson et al., 1987). The precise nature of the pH-dependent change in the $[3Fe\text{-}4S]^0$ cluster remains mysterious. The large change in MCD demonstrates a major change in the electronic structure of the cluster on (de)protonation. However, the site of (de)protonation and the degree to which the geometry of the cluster and its environment is modified are unknown. It is not even clear whether or not the ground-state spin-state of the acid form of the $[3Fe\text{-}4S]^0$ cluster is the same as that of the alkaline cluster. In addition to the uncertainties regarding the $[3Fe\text{-}4S]^0$ cluster, the structures of the products of $Fe(CN)_6^{3-}$ oxidation of FdI remain incompletely characterized. Our previous analyses of this process based on the earlier X-ray structure of FdI require revision. We are therefore continuing spectroscopic, crystallographic, and chemical studies of FdI. Recently, cloning, sequencing, and mutant analysis of the gene encoding FdI have been accomplished (Morgan et al., 1988; Martin et al., 1989), and studies of FdI modified by means of site-directed mutagenesis have been initiated. The purification and structural characterization by X-ray crystallography of (Cys20 → Ala)FdI have already been reported (Martin et al., 1990). In this paper, we focus on the UV–visible absorption, CD, MCD, and EPR spectra of native FdI in its oxidized and DT-reduced states. We demonstrate the observability of the pH dependence of the $[3Fe\text{-}4S]^0$ cluster via natural CD (at room temperature in the absence of glassing agents) in addition to MCD (at low temperature in the presence of glassing agents). We present thorough studies of the MCD of FdI in both oxidized and DT-reduced states. We show that *both* the novel acid form of the $[3Fe\text{-}4S]^0$ cluster and the alkaline form possess $S \geq 2$ ground states.

Experimental Procedures

Purification of FdI. All FdI used in the studies described in this paper was purified according to one of three procedures. All three procedures were carried out aerobically, unless otherwise indicated. Following purification by one of the methods described below, FdI was crystallized and redissolved in 0.1 M potassium phosphate buffer, pH 7.4 or 7.5. A_{280}/A_{400} and A_{280}/A_{260} ratios were 1.6–1.7 and 1.22–1.27, respectively.

Method 1. This method is a modification of that reported by Shethna (1970). *A. vinelandii* (strain OP, ATCC No. 13705) was grown on Burk's N-free medium at 30 °C for 18–24 h in a 500-L fermentor. The cell paste was harvested by centrifugation, washed with 0.05 M potassium phosphate (pH 7.4), and stored frozen at −18 °C until needed. All purification steps were carried out at 2 °C.

The cells were lysed by mixing 1 kg of frozen cell paste, 1 L of 0.05 M potassium phosphate (pH 7.4), and 1 L of 1-butanol for 4 min in a Waring blender. The mixture was then centrifuged at 9000*g* for 45 min in a Beckman J2-21 centrifuge, the butanol layer was discarded, and the aqueous layer (dark green-brown) was decanted. The remaining pellet was then reextracted as just described, and the pooled aqueous extracts were centrifuged at 9000*g* for 45 min to remove remaining debris. The supernatant was then mixed with 50 g of DE-52 (diethylaminoethyl)cellulose (Whatman, equilibrated in 0.05 M potassium phosphate, pH 7.4). After being stirred for 4 h, the DE-52 cellulose was either filtered or collected by centrifugation (3000*g*, 15 min) and then washed with 6 volumes of 0.05 M potassium phosphate (pH 7.4). The greenish DE-52 cellulose was suspended in the same buffer and poured into a 5.2 × 34 cm column. A fraction containing FdI and flavodoxin was eluted batchwise in ~100 mL of 0.1 M potassium phosphate buffer (pH 7.4), 0.3 M in KCl. This fraction was then concentrated and dialyzed by ultrafiltration (Amicon, UM-2 membrane) against 0.025 M potassium phosphate (pH 7.4). The concentrate was applied to a 2.6 × 40 cm DE-52 cellulose column equilibrated with 0.05 M potassium phosphate buffer (pH 7.4). The column was then sequentially washed with (a) a 0.05–0.1 M potassium phosphate (pH 7.4) linear gradient (500 mL of each); (b) a 0–0.12 M KCl linear gradient (500 mL of each) in 0.1 M potassium phosphate (pH 7.4); and (c) 6 L of 0.1 M potassium phosphate (pH 7.4), 0.12 M in KCl. The dark brown FdI band was then eluted with a 0.12–0.3 M KCl linear gradient (500 mL of each) in 0.1 M potassium phosphate (pH 7.4).

Fractions with $A_{280}/A_{400} \leq 4.0$ were pooled, concentrated by ultrafiltration to ~5 mL (Amicon, UM-2), and applied to a 1.6 × 60 cm Sephadex G-75 superfine column run in 0.05 M potassium phosphate (pH 7.4). The column separated a minor yellow impurity of higher molecular weight. FdI fractions with $A_{280}/A_{400} \leq 2.0$ were pooled and concentrated to $A_{400} \sim 2$. Solid $(NH_4)_2SO_4$ was added with stirring to the protein on ice until saturated. The mixture was stored at −18 °C for 12 to 24 h. The flocculent brown FdI precipitate was

collected by centrifugation at 10000*g* for 10 min. The supernatant of this treatment is colorless. Total yield was 7–10 mg of FdI/kg of cells. Dissolved, $(NH_4)_2SO_4$-precipitated FdI generally exhibited A_{280}/A_{400} in the range 1.7–1.9; the lowest value observed was 1.64; for this sample A_{280}/A_{260} was 1.27.

Method 2. A. vinelandii was grown, and cell-free extracts were prepared and heat treated exactly as described for the purification of nitrogenase (Burgess et al., 1980). The heat-treated cell-free extracts were loaded on a 5 × 10 cm DE-52 cellulose column equilibrated with 0.025 M Tris-HCl (pH 7.4), 0.1 M in NaCl, and 1 mM in DT. This column was then developed with a 0.1–0.5 M NaCl linear gradient (1200 mL of each, 400 mL/h) in 0.025 M Tris-HCl (pH 7.4, 1 mM DT). The column effluent was monitored spectrophotometrically at 405 nm. Following the elution of MoFe- and Fe-proteins, an A_{405} peak corresponding to FdI was observed at about 0.4 M NaCl. All of these procedures were carried out anaerobically. FdI was collected aerobically and stored at −20 °C. Fractions were then pooled and concentrated on a 2.7 × 7 cm DE-52 cellulose column equilibrated with 0.025 M Tris-HCl (pH 7.4) and eluted with 0.5 M NaCl in the same buffer.

Accumulated concentrated fractions containing 20–50 mg of FdI were then dialyzed by ultrafiltration (Amicon, UM-2) against 0.05 M potassium phosphate (pH 7.4) and applied to a 2.6 × 40 cm DE-52 cellulose column equilibrated with 0.1 M potassium phosphate (pH 7.4). The column was washed sequentially with a 0.02–0.12 M KCl linear gradient (500 mL of each) in 0.1 M potassium phosphate buffer (pH 7.4) followed by 4 L of 0.12 M KCl in the same buffer. FdI was eluted with a 0.12–0.3 M KCl linear gradient (500 mL of each) in 0.1 M potassium phosphate (pH 7.4). Fractions with $A_{280}/A_{400} \leq 3.5$ were pooled, dialyzed and concentrated by ultrafiltration (Amicon, UM-2) against 0.1 M glycine hydrochloride (pH 8.0), and applied to a DE-52 cellulose column (2.6 × 40 cm) equilibrated with 0.1 M glycine hydrochloride (pH 8.0). FdI was eluted with a 0–0.4 M NaCl gradient (500 mL of each) in the same buffer. FdI fractions with $A_{280}/A_{400} \leq 2.5$ were pooled, concentrated by ultrafiltration (Amicon, UM-2) against 0.1 M potassium phosphate (pH 7.4), and applied to a 1.5 × 60 cm Sephadex G-75 superfine column equilibrated in 0.05 M potassium phosphate (pH 7.4). FdI fractions with $A_{280}/A_{400} \leq 2.0$ were pooled, concentrated, and precipitated with $(NH_4)_2SO_4$ as in method 1. The dissolved, $(NH_4)_2SO_4$-precipitated FdI had A_{280}/A_{400} and A_{280}/A_{260} ratios comparable to those obtained by method 1. The lowest A_{280}/A_{400} ratio was 1.72; for this sample A_{280}/A_{260} was 1.23.

Method 3. This method is a simplification of method 2 and, as with that method, used accumulated partially purified FdI from nitrogenase preparations as the starting material. This protein (20–50 mg) was loaded onto a 2.5 × 25 cm DE-52 cellulose column preequilibrated with 0.1 M potassium phosphate (pH 7.4). The column was washed with 5 L of 0.12 M KCl and developed with a 0.12–0.3 M KCl linear gradient (500 mL of each), and FdI was eluted with additional 0.3 M KCl, all KCl solutions being in 0.1 M potassium phosphate buffer (pH 7.4). The protein was diluted and loaded onto a final 2.5 × 25 cm DE-52 cellulose column equilibrated with 0.1 M glycine hydrochloride (pH 8.0). After washing with the loading buffer, the column was developed with a 0–0.4 M NaCl linear gradient (500 mL of each) and the FdI eluted with additional 0.4 M NaCl, all in 0.1 M glycine (pH 8.0). The FdI was concentrated (Amicon, YM-2) and loaded onto a 100 × 2.4 cm Sephadex G-75 column in 0.1 M potassium phosphate (pH 7.4). FdI fractions with $A_{280}/A_{400} \leq 2.0$ were pooled and precipitated with $(NH_4)_2SO_4$ as in methods 1 and 2. The dissolved, $(NH_4)_2SO_4$-precipitated FdI had A_{280}/A_{400} and A_{280}/A_{260} ratios comparable to those obtained by methods 1 and 2. The lowest A_{280}/A_{400} ratio was 1.74; for this sample A_{280}/A_{260} was 1.25.

Crystallization. FdI was crystallized in tetragonal and triclinic forms as previously described (Stout, 1979). Crystallization and diffraction patterns of triclinic and tetragonal crystals were essentially identical for FdI purified according to methods 1, 2, and 3.

Spectroscopy. All spectroscopic studies were carried out with FdI in 0.1 M potassium phosphate buffer, pH 7.4, or 7.5 or in a mixture of 50 mM PIPES and 50 mM TAPS buffers at pH 6.0, 6.8, 7.5, 8.3, or 9.0. All samples were prepared anaerobically under N_2 in a Vacuum Atmospheres glove box ($O_2 < 1$ ppm). Samples purified aerobically as described above were diafiltered with deaerated potassium phosphate buffer in an Amicon cell with a YM-5 membrane. This procedure also adjusted the concentration of FdI to the desired level. Alternatively, stock FdI in 0.1 M potassium phosphate buffer (pH 7.4) was concentrated to the desired level in a Centricon-10 microconcentrator and exchanged into deaerated 50 mM PIPES/50 mM TAPS buffer of the desired pH by passage through small Sephadex G-25 columns preequilibrated in the buffer. These columns were made from 3-mL disposable syringes (Monoject) and Teflon fritted discs. Prior to loading the FdI, the columns were centrifuged almost to dryness in a clinical centrifuge (International Equipment Corp.) for 1.5 min at 300 rpm. After 300–400 μL of protein solution was loaded, the columns were again centrifuged for 1.5 min, and the buffer exchanged FdI collected. Reduction of FdI was carried out by addition of DT to 2 mM and incubation until no change in absorption at $\lambda \geq 350$ nm could be observed (~20 min) except in the case of MCD samples, where DT was added to 25 mM. Absorption, CD, and EPR spectroscopies were generally carried out with solutions in the concentration range 10^{-5}–10^{-4} M. MCD studies required higher concentrations (10^{-4}–10^{-3} M).

Near-IR–visible–near-UV absorption and CD spectra were obtained over the range 200–900 nm and at ambient temperatures using a Cary 17 spectrometer and a JASCO J-500C spectropolarimeter, respectively. Samples were loaded inside the glove box into small cylindrical cells with fused quartz windows (Optical Cell Co.), which in turn were placed into o-ring-sealed holders with fused quartz windows.

Near-IR–visible–near-UV MCD spectra were obtained over wavelength, temperature, and magnetic field (H) ranges of 200–900 nm, 1.6–60 K, and 0–3.0 T, respectively, using a JASCO J-500C spectropolarimeter and an Oxford Instruments SM5 split-coil superconducting magnet system (Devlin, Morgan, and Stephens, unpublished results). Inside the glove box, MCD samples were first diluted with deaerated glycerol or ethylene glycol (Aldrich), ~50% v/v, then loaded into a cell containing two fused quartz windows separated by an ~1-mm rubber gasket. Cells were then either frozen in liquid nitrogen and, immediately prior to study, transferred under liquid nitrogen to the sample probe and rapidly inserted into the helium-filled sample insert of the SM5 or directly transferred to the probe and frozen in the SM5. In the case of samples reduced by DT, the glycerol or ethylene glycol added also contained DT. In all cases, the room temperature absorption and CD of the samples were measured before and after addition of glycerol or ethylene glycol, prior to loading the MCD cell. In no case was any change in shape detected. Changes in intensity were used to measure accurately the

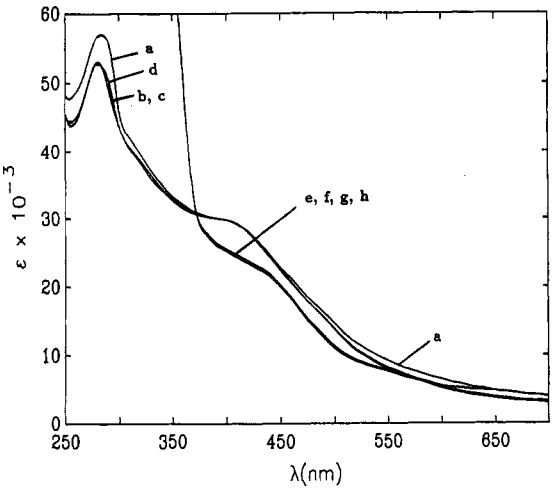

FIGURE 1: Absorption spectra of FdI_{ox} (a–d) and FdI_{red} (e–h): (a) in 100 mM potassium phosphate buffer; (b–h) in 50 mM PIPES/50 mM TAPS buffer. (a) pH = 7.4, (b) pH = 6.0, (c) pH = 7.5, (d) pH = 9.0, (e) pH = 6.0, (f) pH = 6.8, (g) pH = 7.5, and (h) pH = 8.3. Spectra (e–h) were in 2 mM sodium dithionite. The concentration of FdI was in the range 40–65 μM.

dilution caused by addition of glycerol or ethylene glycol. Strain in samples, mounted in the magnet at zero field and low temperature, was monitored by comparing the CD of solutions containing $NiSO_4$ and potassium *d*-tartrate placed before and after the magnet. In no case was significant strain detected.

Absorption, CD, and MCD data are reported in terms of absorbance, A, and differential absorbance, $\Delta A = A_L - A_R$, or molar extinction coefficient, ϵ, and differential molar extinction coefficient, $\Delta\epsilon = \epsilon_L - \epsilon_R$. Beer's Law is assumed throughout. Concentrations of oxidized FdI solutions were obtained by using $\epsilon_{400} = 29800\ M^{-1}\ cm^{-1}$ [based on amino acid analysis; W. V. Sweeney, private communication (1982)]. We assume no change in ϵ_{400} on addition of glycerol or ethylene glycol. Path lengths of MCD cells are obtained at room temperature by both direct measurement (with a micrometer) and by absorption and CD spectroscopy (with a fixed pathlength cell as a reference). We ignore changes in concentration and path length on freezing MCD cells.

Liquid helium temperature EPR spectra were obtained by using a Bruker ER-200D spectrometer and an Oxford Instruments ESR-900 flow cryostat. Samples were placed in cylindrical quartz tubes, which, after sealing with a septum and removal from the glove box, were rapidly frozen in liquid nitrogen. Integration of EPR spectra was carried out by using CuEDTA (1 mM) as a standard. All EPR tubes were calibrated at room temperature using 4-hydroxy-2,2,6,6-tetramethylpiperidinyl-*N*-oxyl (a gift from Professor L. A. Singer).

Results and Discussion

The near-IR–visible–near-UV absorption and CD spectra of as-isolated, air-oxidized FdI (henceforth FdI_{ox}) over the pH range 6.0–9.0 and in both PIPES/TAPS and potassium phosphate buffers are presented in Figures 1 and 2. There is no detectable change in shape with pH in either absorption or CD spectra. At wavelengths $\geq$ 300 nm, absorption and CD are attributable to the Fe-S clusters of FdI_{ox}. We infer that no structural changes in FdI_{ox} significantly affecting its Fe-S clusters occur over the pH range 6.0–9.0.

Addition of DT to FdI_{ox} causes bleaching of the absorption and major change in the CD. Absorption and CD spectra obtained over the pH range 6.0–8.3 in the presence of 2 mM DT and in PIPES/TAPS buffer are shown in Figures 1 and

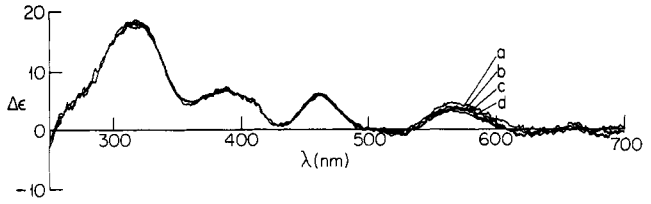

FIGURE 2: CD spectra of FdI_{ox}. FdI solutions were (a) in 100 mM potassium phosphate buffer and (b–d) in 50 mM PIPES/50 mM TAPS buffer. (a) pH = 7.4, (b) pH = 6.0, (c) pH = 7.5, and (d) pH = 9.0.

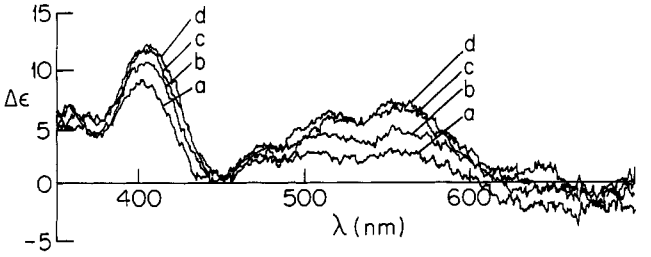

FIGURE 3: CD spectra of FdI_{red}. All samples were in 50 mM PIPES/50 mM TAPS buffer and contained 2 mM DT. (a) pH = 6.0, (b) pH = 6.8, (c) pH = 8.3, and (d) pH = 7.5.

3. CD spectra measured on progressive addition of DT at a single pH value exhibited clean isosbestic points, implicating a single reduction product, FdI_{red}. After addition of a large excess of DT, absorption and CD spectra are stable over several hours (excepting UV absorption changes attributable to DT decomposition). While the absorption spectrum of FdI_{red} is insensitive to pH, a significant variation of CD with pH is observed, indicating some protonation–deprotonation of FdI_{red} significantly affecting one or both of the Fe-S clusters within the pH range studied. Spectra of FdI_{red} are not reported at pH > 8.3 since at pH $\geq$ 8.5 DT causes complex, time-dependent changes in absorption and CD spectra (Stephens et al., 1986).

The EPR of FdI_{ox} at ~10 K is nearly isotropic, with $g \sim 2.01$, and narrow. With increasing temperature, the EPR broadens rapidly and above ~30 K is undetectable. The EPR at ~10 K over the pH range 6.0–9.0 and in both PIPES/TAPS and potassium phosphate buffers is presented in Figure 4. Like the absorption and CD spectra, the EPR is insensitive to pH. Integration of the EPR at ~10 K yields ~1 spin/molecule. The EPR of FdI_{ox} is attributable to the $[3Fe\text{-}4S]^{1+}$ cluster (Emptage et al., 1980); the $[4Fe\text{-}4S]^{2+}$ cluster is EPR silent. The EPR spectra confirms that no structural change in FdI_{ox} significantly affecting the $[3Fe\text{-}4S]^{1+}$ cluster occurs over the pH range 6.0–9.0.

Addition of excess DT to FdI_{ox} at pH = 8.3 causes nearly complete loss of the EPR of FdI_{ox}, without appearance of any new signal, as shown in Figure 4. Over the pH range 6.0–8.3, the intensity of the residual FdI_{ox} signal varies with pH, increasing with decreasing pH (presumably as a result of the increasing reducing power of dithionite with increasing pH; note that the pH dependence of the $[3Fe\text{-}4S]^{1+/0}$ redox potential (Armstrong et al., 1988) would lead to an opposite result). At pH 6.0 and 8.3, the spectra in Figure 4 yield 10% and 1% residual FdI_{ox}, respectively. The variable presence of these quantities of FdI_{ox} in these samples is not sufficient to account for the observed pH dependence of the CD of FdI_{red}. Again, the spectra of DT-reduced FdI_{ox} are limited here to the range 6.0–8.3. At pH $\geq$ 8.5, more complex and time-dependent EPR spectra are observed (including more than one $g \sim 1.94$ signal) (Stephens et al., 1986). The disappearance of the $g \sim 2.01$ EPR and the nonappearance of $g \sim 1.94$ EPR

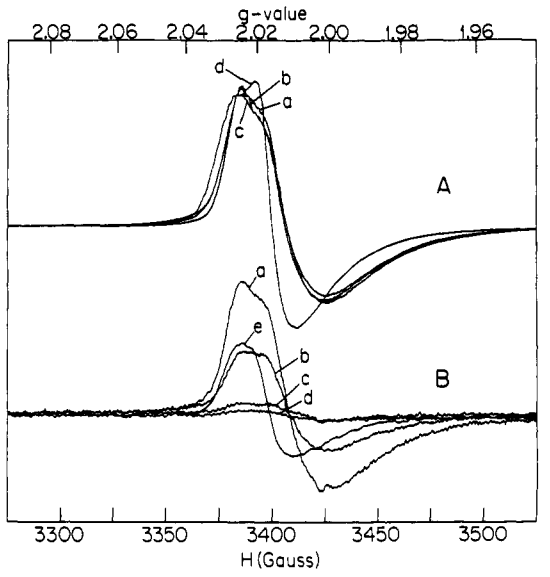

FIGURE 4: EPR spectra of (A) FdI_{ox} and (B) FdI_{red}. All spectra were recorded at ~10 K, 1-mW microwave power, 5-G modulation amplitude, and 9.59-GHz microwave frequency. (A) (a) pH = 6.0, (b) pH = 7.5, and (c) pH 9.0, all in 50 mM PIPES/50 mM TAPS buffer; (d) pH = 7.4 in 100 mM potassium phosphate buffer. The spectra in (A) have been normalized to constant integrated intensity. (B) (a) pH = 6.0, (b) pH = 6.8, (c) pH = 7.5, and (d) pH = 8.3, all in 50 mM PIPES/50 mM TAPS buffer; (e) pH = 7.4 in 100 mM potassium phosphate buffer. The spectra in (B) have been normalized with respect to gain, protein concentration, and tube size.

over the pH range 6.0–8.3 shows that DT reduction of FdI_{ox} to FdI_{red} involves reduction of the $[3Fe\text{-}4S]^{1+}$ cluster to $[3Fe\text{-}4S]^{0}$ without reduction of the $[4Fe\text{-}4S]^{2+}$ cluster. [The possibility of reduction to an EPR silent $[4Fe\text{-}4S]^{1+}$ cluster is ruled out by the earlier studies by Mössbauer spectroscopy (Emptage et al., 1980).] Since there is pH dependence in the CD spectrum of FdI_{red}, but not FdI_{ox}, it is reasonable to infer thence that the (de)protonation of FdI_{red} affects primarily, and occurs at or near, the $[3Fe\text{-}4S]^{0}$ cluster.

Figure 5 presents low temperature near-IR–visible–near-UV MCD spectra of FdI_{ox} in potassium phosphate buffer, pH 7.5, diluted ~50% v/v by glycerol. Room temperature absorption and CD spectra of FdI_{ox} before and after addition of glycerol were superimposable, showing that glycerol does not cause any structural change in FdI_{ox} significantly affecting its Fe-S clusters. The MCD spectra show paramagnetic behavior, decreasing with increasing temperature (Stephens, 1976). The field dependence at several temperatures and the temperature dependence up to ~60 K at low, nonsaturating fields at several wavelengths are presented in Figures 6 and 7. As shown in Figure 6, the field dependence of the MCD at all temperatures and wavelengths measured can be accurately fit to the functional form appropriate to an $S = {}^1/_2$ ground state with an isotropic g-tensor (Stephens, 1976):

$$\Delta A = (\Delta A_0) \tanh\left(\frac{g\beta H}{2kT}\right) \qquad (1)$$

with $g = 2.01$. As shown in Figure 7, the temperature dependence of the MCD, measured at fields low enough to avoid significant field saturation, at all wavelengths studied is accurately linear in $1/T$ up to ~60 K, demonstrating the absence, up to ~60 K, of significant population of any excited electronic state. The field saturation identifies the ground state from which the MCD originates with the $S = {}^1/_2$, $g \sim 2.01$ level responsible for the EPR. The paramagnetic MCD thus arises from the $[3Fe\text{-}4S]^{1+}$ cluster.

Low temperature MCD spectra of FdI_{red} at pH 8.3 and 6.0 are presented in Figures 8 and 11. FdI_{red} was in PIPES/TAPS buffer and diluted by ethylene glycol ~50% v/v. At each pH, ethylene glycol was shown to cause negligible change in the absorption and CD of FdI_{red}, indicating a negligible effect of the glassing agent on the Fe-S clusters in FdI_{red}. In particular, the equilibrium between protonated and deprotonated forms of FdI_{red} is not affected by ethylene glycol. EPR spectra of samples used for MCD spectroscopy showed residual FdI_{ox} EPR quantitating to 10% and 3% at pH 6.0 and 8.3, respectively.

The MCD spectra of FdI_{red} at pH 6.0 and 8.3 are both predominantly paramagnetic, decreasing with increasing temperature. The spectra are very different in shape (wavelength dependence) however. Measurements of the field dependence at selected temperatures and wavelengths are presented in Figures 9 and 12. Measurements of the temperature dependence at nonsaturating fields at selected wavelengths up to ~50 K are presented in Figures 10 and 13. In the case of the pH 6.0 spectra, in view of the substantially greater FdI_{ox} concentration present, the wavelengths used for studying field dependence and temperature dependence are selected to be wavelengths at which FdI_{ox} MCD is zero. Figure 9 shows rapid saturation with increasing field, varying in form with temperature at all wavelengths studied, behavior referred to as "nesting" (Thomson & Johnson, 1980). Figure 12 exhibits qualitatively similar behavior. It follows that at both pH 6.0 and 8.3, the MCD of FdI_{red} originates in a paramagnetic ground state of $S > {}^1/_2$, exhibiting zero-field splitting. Since the [4Fe-4S] cluster in FdI_{red} is in the EPR silent,

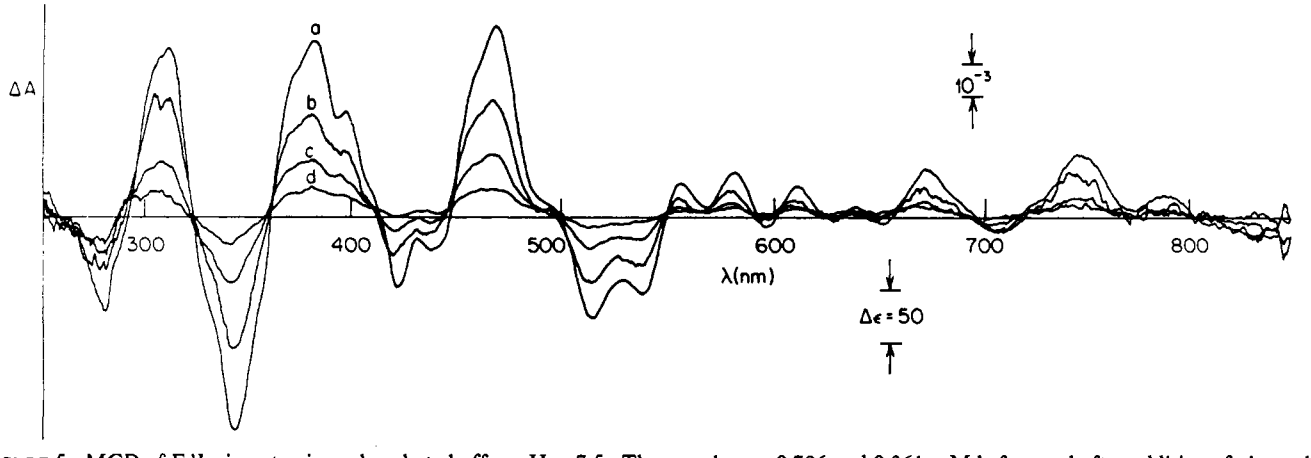

FIGURE 5: MCD of FdI_{ox} in potassium phosphate buffer, pH = 7.5. The sample was 0.706 and 0.361 mM before and after addition of glycerol. The path length was 0.96 mm. Temperatures were (a) 1.76 K, (b) 3.53 K, (c) 7.64 K, and (d) 19.6 K. Magnetic field was 3.00 T.

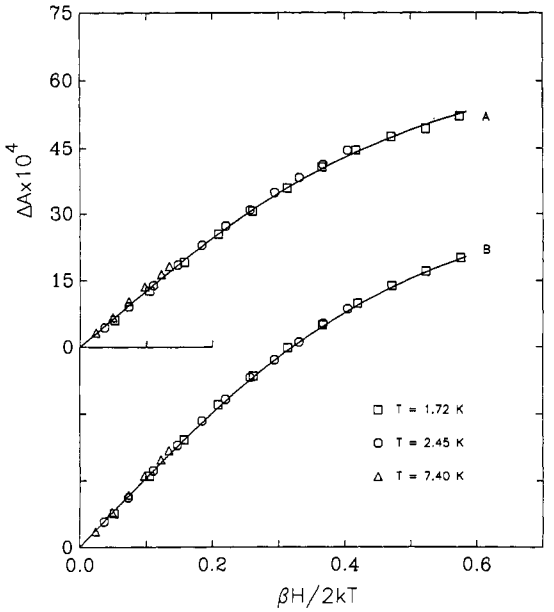

FIGURE 6: Field dependence of the MCD of FdI_{ox}. Temperatures are as indicated. Wavelengths are (A) 469 nm and (B) 343 nm. The sample is as in Figure 5. The lines are calculated from eq 1, with $g = 2.01$.

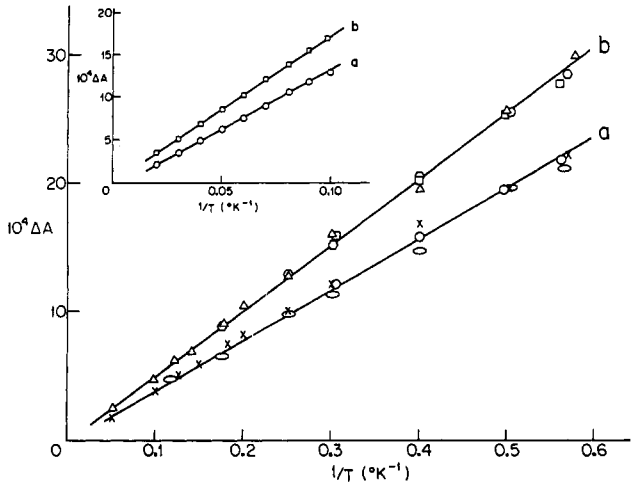

FIGURE 7: Temperature dependence of the MCD of FdI_{ox} over the range 1.7–60 K. (a) and (b) show differences in MCD from 470 to 515 nm and from 383 to 344 nm, respectively. The results of three separate experiments are shown; different experiments are normalized at 2.00 K. All data were measured at fields below the threshold for saturation and are normalized to $H = +0.938$ T. In the inset, data over the range 10–60 K are shown, normalized to $H = +2.34$ T. FdI_{ox} samples were 0.17–0.29 mM, after addition of 50% v/v glycerol and in potassium phosphate buffer, pH = 7.5. Cell path lengths were ~1 mm.

diamagnetic 2+ oxidation level (Emptage et al., 1980), the MCD of FdI_{red} arises from the $[3Fe\text{-}4S]^0$ cluster. The pH dependence of the MCD of FdI_{red} parallels that observed in the room temperature CD and further confirms that the $[3Fe\text{-}4S]^0$ cluster is affected by the change in pH.

The nature of the ground state of the $[3Fe\text{-}4S]^0$ cluster at pH 6.0 and 8.3 can be determined from the MCD temperature-dependence data presented in Figures 10 and 13. We start from the assumption that the ground state of the $[3Fe\text{-}4S]^0$ cluster is $S = 1$ or $S = 2$; since it is an even electron system, $S \neq 0$ and $S \geq 3$ states are unprecedented. In axial fields, $S = 1$ and $S = 2$ states suffer zero-field splitting. Negative D values lead to the $M_s \pm 1$ and $M_s \pm 2$ levels being lowest for $S = 1$ and $S = 2$, respectively. Positive D values lead to the nondegenerate $M_s = 0$ being lowest in both cases.

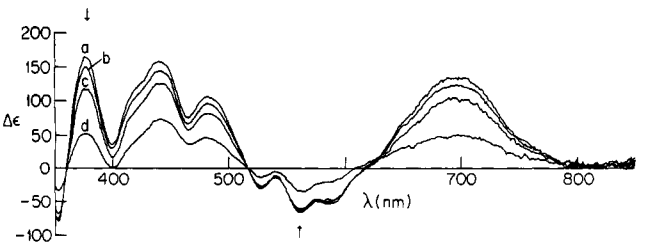

FIGURE 8: MCD of FdI_{red}. FdI_{red} was 0.168 mM in 50 mM PIPES/50 mM TAPS buffer, pH = 8.3, 50% v/v ethylene glycol, and 25 mM sodium dithionite. The path length was 0.94 mm (a) or 1.04 mm (b–d). Temperatures were (a) 1.77 K, (b) 2.00 K, (c) 4.00 K, and (d) 9.98 K. $H = +3.00$ T. The arrows indicate the wavelengths used for theoretical analysis.

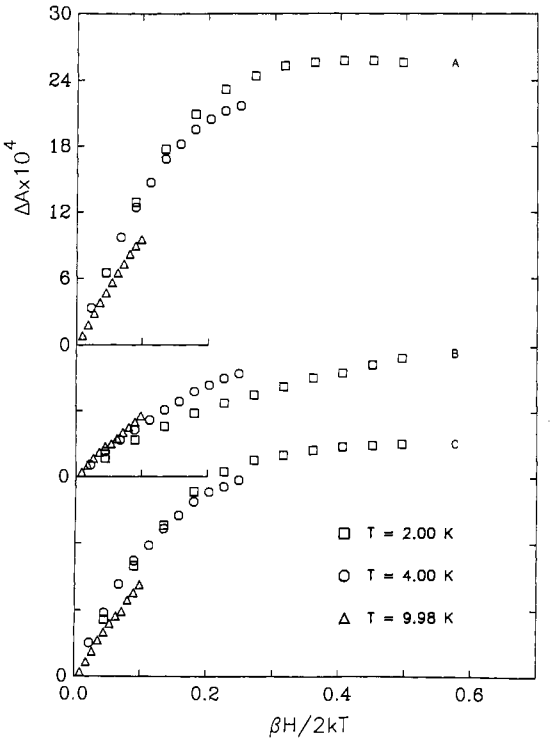

FIGURE 9: Field dependence of the MCD of FdI_{red}. The sample was as in Figure 8. The path length was 1.04 mm. Wavelengths were (A) 378 nm, (B) 563 nm, and (C) 695 nm. Temperatures are as indicated.

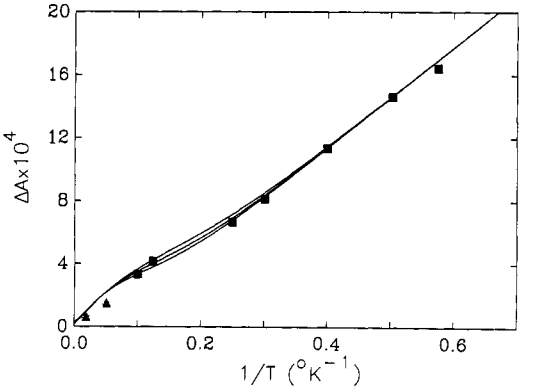

FIGURE 10: Temperature dependence of the MCD (difference from 378 to 563 nm) of FdI_{red} over the range 1.77–50 K. The data were recorded at 0.536 T (■) or at 1.072 T (▲). All data are normalized to 0.536 T. The sample was as in Figure 8. The path length was 0.94 mm. The solid lines are calculated from eq 3 and $D = -3.0$, -3.5, and -4.0 cm^{-1}.

In rhombic fields, M_s is no longer a good quantum number and all degeneracy is lost. The linearity in $1/T$ (within experimental error) of the MCD at the lowest temperatures in

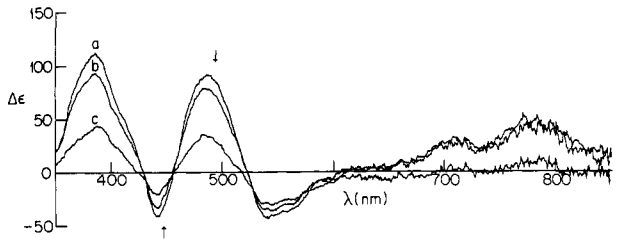

FIGURE 11: MCD of FdI_{red}. FdI_{red} was 0.155 mM in 50 mM PIPES/50 mM TAPS buffer, pH 6.0, 50% v/v ethylene glycol, and 25 mM sodium dithionite. The path length was 0.95 mm. Temperatures were (a) 2.00 K, (b) 4.00 K, and (c) 10.00 K. $H = +3.00$ T. The arrows indicate the wavelengths used for theoretical analysis.

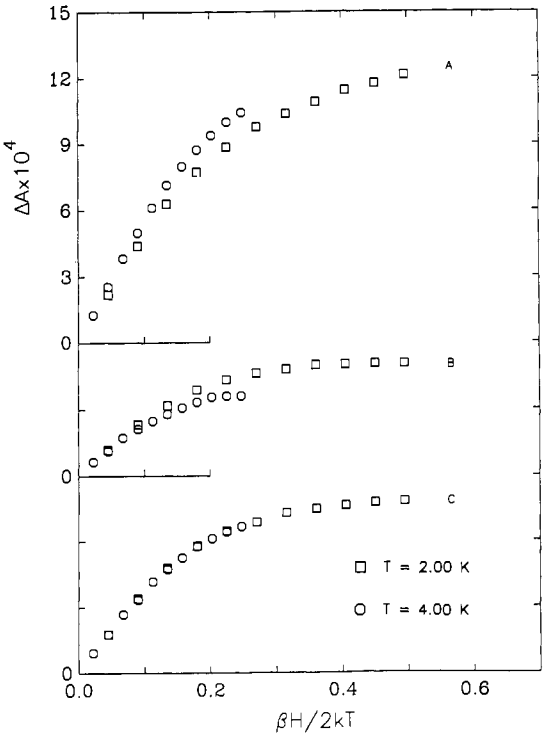

FIGURE 12: Field dependence of the MCD of FdI_{red}. The sample was as in Figure 11. The path length was 0.95 mm. Wavelengths were (A) 496 nm, (B) 449 nm, and (C) 411 nm. Temperatures are as indicated.

Figures 10 and 13 is in both cases consistent with a ground state exactly or very nearly degenerate [in the latter case the splitting must be $\ll 1.77$ K ($=1.24$ cm^{-1}), the lowest temperature at which MCD was measured]. We therefore assume an axial zero-field spin-Hamiltonian, DS_z^2, with $D < 0$ as a good first approximation. At fields sufficiently small to avoid significant field saturation, the MCD arising from $S = 1$ and $S = 2$ ground states can be written (Stephens, 1976) for $S = 1$

$$\Delta A = \gamma\{\alpha_1[B_{10} + B_1 + C_1/kT] + \alpha_0[-B_{10} + B_0]\}\beta H \quad (2)$$

and for $S = 2$

$$\Delta A = \gamma\left\{\alpha_2\left[B_{21} + B_{20} + B_2 + \frac{C_2}{kT}\right] + \alpha_1\left[-B_{21} + B_{10} + B_1 + \frac{C_1}{kT}\right] + \alpha_0[-2B_{20} - 2B_{10} + B_0]\right\}\beta H \quad (3)$$

where α_i is the Boltzmann population of state $M_s = \pm i$, C_i is the C parameter for state $M_s = \pm i$, B_{ij} is the B parameter of state $M_s = \pm i$ arising from mixing with state $M_s = \pm j$, and B_i is the B parameter of the state $M_s = \pm i$ arising from mixing

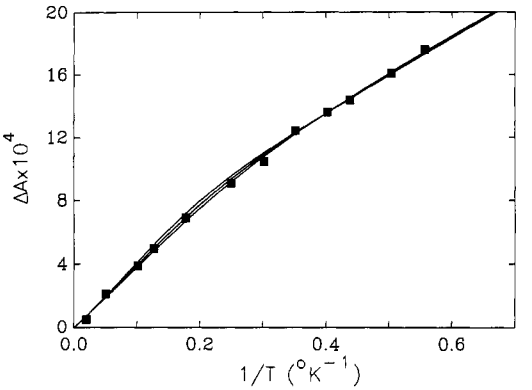

FIGURE 13: Temperature dependence of the MCD (difference from 449 to 496 nm) of FdI_{red} over the range 1.77–50 K and at 0.536 T. The sample was as in Figure 11 except that the concentration of FdI_{red} was 0.183 mM. The path length was 0.97 mm. The solid lines are calculated from eq 3 and $D = -1.5$, -2.0, and -2.5 cm^{-1}.

with all states outside of the ground ($S = 1$ or 2) manifold. Important limits to eq 2 and 3 are for $kT \ll D$ and $S = 1$

$$\Delta A = \gamma\left[B_{10} + B_1 + \frac{C_1}{kT}\right]\beta H \quad (4)$$

and for $kT \ll D$ and $S = 2$

$$\Delta A = \gamma\left[B_{21} + B_{20} + B_2 + \frac{C_2}{kT}\right]\beta H \quad (5)$$

and for $kT \gg D$ and $S = 1$

$$\Delta A = \gamma\left[\frac{2}{3}B_1 + \frac{1}{3}B_0 + \frac{2}{3}\frac{C_1}{kT}\right]\beta H \quad (6)$$

and for $kT \gg D$ and $S = 2$

$$\Delta A = \gamma\left[\frac{2}{5}B_2 + \frac{2}{5}B_1 + \frac{1}{5}B_0 + \frac{2}{5}\frac{(C_1 + C_2)}{kT}\right]\beta H \quad (7)$$

Thus, in both low and high temperature limits, the MCD must be linear in $1/T$. In the case of $S = 1$, the high temperature slope is *always* less than the low temperature slope. In the case of $S = 2$, the high temperature slope may be *either* larger or smaller than the low temperature slope. Returning to Figures 10 and 13, we see that in both cases, for the wavelengths studied, the high temperature slope is *greater* than that at the lowest temperatures. This immediately eliminates $S = 1$ as a possible ground state at both pH 6.0 and 8.3. Quantitative analysis of the MCD data of Figures 10 and 13 using eq 3 permits the axial zero-field splitting parameter, D, to be obtained. Least-squares fitting of the linear low temperature data yields C_2 and $(B_{21} + B_{20} + B_2)$ from the slope and intercept, respectively. Fitting of the linear high temperature data yields $^2/_5(C_1 + C_2)$ and $^1/_5(2B_2 + 2B_1 + B_0)$ from the slope and intercept, respectively. Since at both pH values the high temperature intercept and thus $^1/_5(2B_2 + 2B_1 + B_0)$ is zero (within experimental error), we assume that B_2, B_1, and B_0 are individually zero. The low temperature intercept then yields $(B_{21} + B_{20})$. Further fitting is carried out iteratively. We first assume $B_{20} = B_{10} = 0$ and vary D to obtain an initial estimate of D. For this value of D, B_{10} is then varied to further improve the fit. With the optimum B_{10}, D is in turn varied. Finally, the assumption that $B_{20} = 0$ is relaxed and a final best fit obtained. In the case of the MCD data of Figures 10 and 13, we find that while nonzero values of B_{21} and B_{10} are both mandatory in obtaining acceptable fits, it is unnecessary in practice to allow B_{20} to deviate from zero. The best results obtained with $B_{20} = 0$ are shown in Figures

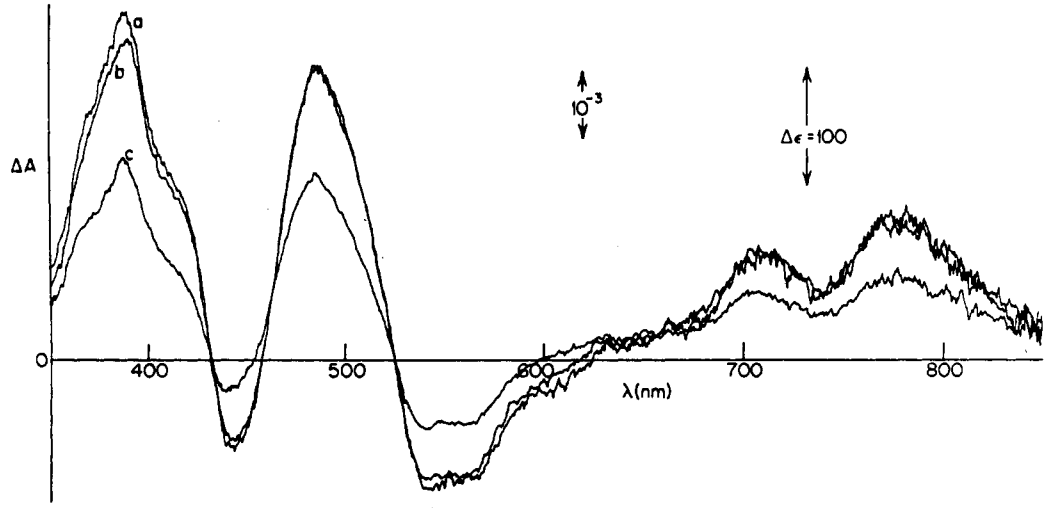

FIGURE 14: MCD of FdI_{red} in potassium phosphate buffer, pH = 7.5. FdI_{red} was 0.382 mM and was diluted by 0.1 M sodium dithionite in 0.1 M Tris buffer, pH = 8.0, to 0.350 mM, giving a [DT]:[FdI] of ~24. After incubation for ~1.5 h, glycerol (to which sufficient dithionite was added to generate an excess) was added, after which FdI_{red} was 0.183 mM. Temperatures and magnetic fields were (a) 1.77 K, +3.00 T; (b) 2.50 K, +3.00 T; (c) 8.00 K, +3.00 T. The path length was 0.98 mm.

10 and 13. At pH 8.3 and 6.0 best fits are achieved with $D = -3.5$ and -2.0 cm^{-1}, respectively. The predictions of eq 3 with identical C_1, C_2, B_{21}, and B_{10} parameters but with D values $+0.5$ cm^{-1} and -0.5 cm^{-1} different are also shown in Figures 10 and 13. Error bars of ± 0.5 cm^{-1} for the D values derived would appear to be realistic.

Our data thus lead to the conclusion that at both pH 6.0 and 8.3 the $[3Fe\text{-}4S]^0$ cluster possesses an $S = 2$ ground state and therefore that the change in MCD with pH does *not* result from a change in spin state *or* from a change in the sign of the zero-field splitting. However, a significant change in the D value is found, showing that the electronic ground state *is* affected by the change in pH. Our data are not inconsistent with $S \geq 3$, but such states are unprecedented, and therefore highly unlikely.

Our earliest studies of the MCD of FdI_{red} were carried out in potassium phosphate buffer, pH 7.5, diluted ~50% v/v by glycerol. The MCD obtained is shown in Figure 14. Comparison to the spectra presented in Figures 8 and 11 shows that the MCD of the phosphate-buffered FdI_{red} is very similar to that of the pH 6.0 PIPES/TAPS-buffered FdI_{red}. This suggests a significant lowering in pH concomitant with freezing to liquid helium temperatures, consistent with the known temperature dependence of the pH of phosphate buffers (Williams-Smith et al., 1977). The same phenomenon is evidenced in Figure 4 for the EPR of FdI_{red} in phosphate and PIPES/TAPS buffers. The presence of the novel acid form of the [3Fe-4S] cluster in phosphate buffer precludes the possibility of a (PIPES) buffer artifact. In our study of the pH dependence of the MCD of FdI_{red}, we have therefore resorted, following George et al. (1984), to the use of buffers whose pH exhibits much smaller temperature dependence. In our initial studies of the MCD of FdI_{ox}, we also employed phosphate buffers. In view of the apparent absence of pH dependence in the properties of FdI_{ox}, we have not repeated our earlier studies of FdI_{ox} using PIPES/TAPS buffers. The phosphate-buffered FdI_{ox} whose MCD is presented in Figures 5–7 presumably suffered a parallel shift in pH to that found in FdI_{red}. [MCD spectra of FdI_{ox} reported by Johnson et al. (1987) in Tris buffer, pH 7.8, appear identical with those in Figure 5.]

The air-oxidized and reduced states of FdI have been characterized by physical techniques in earlier studies. Yoch et al. (1969) reported the near-UV–visible absorption spectra of FdI as isolated and after DT reduction at pH 7.2. EPR spectra of FdI as isolated and after reduction using illuminated chloroplasts at pH 7.4 were reported by Sweeney et al. (1975). Our data are in complete accord with these earlier studies, assuming that illuminated chloroplasts are not capable of reduction of the $[4Fe\text{-}4S]^{2+}$ cluster.

Mössbauer spectroscopy of FdI (Emptage et al. 1980) first identified the $S = {}^1/_2$, $g \sim 2.01$ ground state of the 3Fe cluster and led to the identification of its all-Fe^{3+} oxidation level (Kent et al., 1982). Study of DT-reduced FdI also demonstrated reduction of the 3Fe cluster to a paramagnetic, EPR silent $S \geq 1$ state without concomitant reduction of the $[4Fe\text{-}4S]^{2+}$ cluster, linking the −420 mV midpoint potential to the 3Fe cluster. The pH dependence of the Mössbauer spectra was not reported by Emptage et al. (1980). DT-reduced FdI was studied at pH 9 and presumably contained FdI_{red}, with the $[3Fe\text{-}4S]^0$ cluster in its alkaline form. In view of the complex DT-reduction behavior of FdI at pH ≥ 8.5 subsequently observed by us (Morgan et al., 1984; Stephens et al., 1986), it is surprising that EPR signals, and Mössbauer spectra linked thereto, were not observed. Otherwise, our data and conclusions are completely consistent with these earlier studies.

The near-UV–visible–near-IR CD spectrum of FdI_{ox} at pH 7.5 was first reported by Morgan et al. (1984). The CD of DT-reduced FdI at pH 7.5, together with absorption and CD spectra at pH 9.0, were reported by Stephens et al. (1986). The pH dependence of the CD spectrum of FdI_{red} at pH < 8.5 was not detected in these earlier studies, changes in CD spectra during pH titration (T. V. Morgan, unpublished data) being attributed to the instabilities observed in a pronounced form at pH ≥ 8.5.

Near-UV–visible–near-IR low temperature MCD spectra of FdI_{ox} were first reported by Morgan et al. (1984; 1985) and Stephens et al. (1985). The spectra obtained were recognizably similar to those previously obtained from *Dg*FdII and $Fe(CN)_6^{3-}$-oxidized *Cp*Fd (Thomson et al., 1981a,b). MCD spectra of DT-reduced FdI at pH 7.5 in potassium phosphate buffer were also obtained during those studies. Remarkably, these spectra showed no resemblance to those of DT-reduced *Dg*FdII and $Fe(CN)_6^{3-}$-oxidized *Cp*Fd (Thomson et al., 1981a,b; Beinert & Thomson, 1983). Publication of these data was preempted by the report by George et al. (1984) of a pH dependence in the MCD of reduced *Ac*FdI. The spectrum of the acid form of *Ac*FdI closely resembled that previously

obtained from FdI. The data reported here confirm that the acid and alkaline forms of the [3Fe-4S]^0 cluster exist likewise in FdI. In addition, importantly, the CD data reported here show that this phenomenon also exists at room temperature, in the absence of glassing agents, and does not originate in the addition of glycerol or ethylene glycol or in freezing to 4 K. George et al. (1984) noted the strong similarity of the MCD of the alkaline [3Fe-4S]^0 cluster to that of other [3Fe-4S]^0 clusters. These authors stated, but did not document, that both acid and alkaline [3Fe-4S]^0 clusters have $S = 2$ ground states, the spin state earlier identified for *Dg*FdII (Thomson et al., 1981b). Our studies here provide a firm foundation in support of the same conclusion for FdI.

Subsequent to the report of George et al. (1984), Johnson et al. (1987) studied the MCD of FdI in oxidized and DT-reduced states. Their data for FdI_{ox} replicate our earlier work. Their data for FdI_{red} obtained at pH 6.4 and 8.3 confirm the existence of the pH effect identified by George et al. (1984) in the case of *Ac*FdI. Johnson et al. (1987) further attempted theoretical analyses of the MCD spectra obtained using FdI_{red} in Tris buffer, pH 7.8, and in TAPS buffer, pH 8.5, which resemble those obtained in the present work at pH 8.3. The field dependence of the MCD (in Tris, pH 7.8) at several wavelengths and temperatures, was analyzed assuming an $S = 2$ ground state and axial symmetry, using an ad hoc theoretical approach (Bennett & Johnson, 1987). The temperature dependence of the MCD (in TAPS, pH 8.5) at 690 nm and 0.5 T over the range 4.2–100 K was fit assuming

$$\Delta A = \gamma\left\{\frac{C_2}{kT}\alpha_2 + \frac{C_1}{kT}\alpha_1\right\}\beta H \qquad (8)$$

and $D = -2.0$ (-1.0 to -4.0) cm^{-1} was obtained. Equation 8 is the limit of eq 3 in which all B terms are ignored. Analysis of this type is only valid in an axial system when the electronic transitions are completely polarized perpendicular to the unique axis. This is well known to be the case, for example, for the $\pi \rightarrow \pi^*$ transitions of porphyrins, and an expression of this type was used by Browett et al. (1983) to determine D for the $S = {}^5/_2$ ground state of chloro(*meso*-tetraphenylporphinato)iron(III) from the temperature dependence of its low-field MCD. Johnson et al. (1987) argued that the "predominant" perpendicular polarization at 690 nm deduced from their analysis of the MCD field dependence justified the neglect of B terms. However, the polarization ratio obtained ($m_z/m_{xy} = 0.35$) was not in fact very small and, in any case, resulted from an analysis lacking theoretical foundation. The justifiability of eq 8 is consequently questionable and the D value obtained unlikely to be reliable. In the work reported here, we have eschewed analysis of the MCD field dependence since, in our opinion, a satisfactory formalism for the analysis of the saturation behavior of the MCD of anisotropic systems of effective $S > {}^1/_2$ has yet to be developed. Instead, we have focused our analysis on the temperature dependence of the MCD in the low-field regime, i.e., at fields sufficiently small that the MCD remains linear in field. The theoretical formalism for MCD in this regime is well-known (Stephens, 1970; 1976), permitting reliable data analysis. We have studied the MCD at wavelengths where the dependence on temperature exhibits a substantial deviation from linearity with respect to $1/T$. In this situation, predicted MCD temperature dependence is sensitive to the Boltzmann factors of populated levels, and hence to the zero-field parameters of the ground-state manifold. We have made use of the high and low temperature extremes to demonstrate the utility of the axial zero-field splitting approximation and the inconsistency of the MCD with an $S = 1$ ground-state effective spin. We have shown that the MCD can be fit assuming an axial $S = 2$ ground state and that the fit is sensitive to all of the theoretical parameters entering into the fit, resulting in relatively narrow ranges of possible values. Although Johnson et al. (1987) made use of low-field MCD data, at the wavelength selected the nonlinearity with respect to $1/T$ was not great and the high temperature slope was less than the low temperature slope. These data thus neither permit the identification of the ground-state spin nor facilitate the extraction of the zero-field splitting parameter. The use of eq 8, rather than eq 3, further degrades the reliability of the analysis. Johnson et al. (1987) made no attempt to analyze the MCD spectrum of the acid form of the [3Fe-4S]^0 cluster and concluded only that "the data are indicative of a ground state with $S = 1$ or 2".

In summary, our work thus provides the first analysis of the MCD of the acid form of the [3Fe-4S]^0 cluster and the first *reliable* analysis of the MCD of the alkaline form of the [3Fe-4S]^0 cluster in either FdI or *Ac*FdI.

Spectroscopic and electrochemical studies of other Fe-S proteins containing [3Fe-4S] clusters have not identified pH-dependent [3Fe-4S] cluster properties thus far. The MCD of [3Fe-4S] clusters in *Dg*FdII, *Thermus thermophilus* Fd, and *Pyrococcus furiosus* Fd do not exhibit significant pH dependence (George et al., 1984; Johnson et al., 1987; Conover et al., 1990), and at this time the pH-dependent behavior of the [3Fe-4S]^0 clusters of FdI and *Ac*FdI is unique. The structural basis of the observed changes in spectra and redox potential with pH remains to be established. Since other proteins containing pH-independent [3Fe-4S]^0 clusters show the same MCD as the alkaline form of the [3Fe-4S]^0 cluster in FdI, it can be concluded that the alkaline form of the [3Fe-4S]^0 cluster in FdI is obtained by reduction without protonation or deprotonation of the [3Fe-4S]$^{1+}$ cluster and, consequently, that the acid form of the [3Fe-4S]^0 cluster is more highly protonated than the [3Fe-4S]$^{1+}$ cluster. Reduction with or without protonation may or may not cause measurable structural changes in the [3Fe-4S] cluster and/or its surroundings. The study of FdI by X-ray crystallography, to date exclusively for FdI_{ox}, is currently being extended to include the DT-reduced states to examine whether structural changes are detectable. In addition, the creation of site-directed mutants of FdI and the study of the pH dependence of their [3Fe-4S]^0 clusters is also planned.

References

Adman, E. T., Sieker, L. C., & Jensen, L. H. (1976) *J. Biol. Chem. 251*, 3801–3806.

Armstrong, F. A., George, S. J., Thomson, A. J., & Yates, M. G. (1988) *FEBS Lett. 234*, 107–110.

Beinert, H., & Thomson, A. J. (1983) *Arch. Biochem. Biophys. 222*, 333–361.

Bennett, D. E., & Johnson, M. K. (1987) *Biochim. Biophys. Acta 911*, 71–80.

Browett, W. R., Fucaloro, A. F., Morgan, T. V., & Stephens, P. J. (1983) *J. Am. Chem. Soc. 105*, 1868–1872.

Burgess, B. K., Jacobs, D. B., & Stiefel, E. I. (1980) *Biochim. Biophys. Acta 614*, 196–209.

Conover, R. C., Kowal, A. T., Fu, W., Park, J. B., Aono, S., Adams, M. W. W., & Johnson, M. K. (1990) *J. Biol. Chem. 265*, 8533–8541.

Emptage, M. H., Kent, T. A., Huynh, B. H., Rawlings, J., Orme-Johnson, W. H., & Münck, E. (1980) *J. Biol. Chem. 255*, 1793–1796.

Freer, S. T., Alden, R. A., Carter, C. W., & Kraut, J. (1975) *J. Biol. Chem. 250*, 46–54.

George, S. J., Richards, A. J. M., Thomson, A. J., & Yates, M. G. (1984) *Biochem. J. 224*, 247–251.
Ghosh, D., Furey, W., O'Donnell, S., & Stout, C. D. (1981) *J. Biol. Chem. 256*, 4185–4192.
Ghosh, D., O'Donnell, S., Furey, W., Robbins, A. H., & Stout, C. D. (1982) *J. Mol. Biol. 158*, 73–109.
Howard, J. B., Lorsbach, T. W., Ghosh, D., Melis, K., & Stout, C. D. (1983) *J. Biol. Chem. 258*, 508–522.
Johnson, M. K., Bennett, D. E., Fee, J. A., & Sweeney, W. V. (1987) *Biochim. Biophys. Acta 911*, 81–94.
Kent, T. A., Dreyer, J.-L., Kennedy, M. C., Huynh, B. H., Emptage, M. H., Beinert, H., & Münck, E. (1982) *Proc. Natl. Acad. Sci. U.S.A. 79*, 1096–1100.
Kissinger, C. R., Adman, E. T., Sieker, L. C., & Jensen, L. H. (1988) *J. Am. Chem. Soc. 110*, 8721–8723.
Kissinger, C. R., Adman, E. T., Sieker, L. C., Jensen, L. H., & LeGall, J. (1989) *FEBS Lett. 244*, 447–450.
Martin, A. E., Burgess, B. K., Iismaa, S. E., Smartt, C. T., Jacobsen, M. R., & Dean, D. R. (1989) *J. Bacteriol. 171*, 3162–3167.
Martin, A. E., Burgess, B. K., Stout, C. D., Cash, V. L., Dean, D. R., Jensen, G. M., & Stephens, P. J. (1990) *Proc. Natl. Acad. Sci. U.S.A. 87*, 598–602.
Morgan, T. V., Stephens, P. J., Devlin, F., Stout, C. D., Melis, K. A., & Burgess, B. K. (1984) *Proc. Natl. Acad. Sci. U.S.A. 81*, 1931–1935.
Morgan, T. V., Stephens, P. J., Devlin, F., Burgess, B. K., & Stout, C. D. (1985) *FEBS Lett. 183*, 206–210.
Morgan, T. V., Lundell, D. J., & Burgess, B. K. (1988) *J. Biol. Chem. 263*, 1370–1375.
Robbins, A. H., & Stout, C. D. (1989a) *Proc. Natl. Acad. Sci. U.S.A. 86*, 3639–3643.
Robbins, A. H., & Stout, C. D. (1989b) *Proteins 5*, 289–312.
Shethna, Y. I. (1970) *Biochim. Biophys. Acta 205*, 58–62.
Stephens, P. J. (1970) *J. Chem. Phys. 52*, 3489–3516.
Stephens, P. J. (1976) *Adv. Chem. Phys. 35*, 197–264.
Stephens, P. J., Morgan, T. V., Devlin, F., Penner-Hahn, J. E., Hodgson, K. O., Scott, R. A., Stout, C. D., & Burgess, B. K. (1985) *Proc. Natl. Acad. Sci. U.S.A. 82*, 5661–5665.
Stephens, P. J., Morgan, T. V., Stout, C. D., & Burgess, B. K. (1986) in *Frontiers in Bioinorganic Chemistry* (Xavier, A. V., Ed.) pp 637–646, VCH, Weinheim, FRG.
Stout, C. D. (1979) *J. Biol. Chem. 254*, 3598–3599.
Stout, C. D. (1988) *J. Biol. Chem. 263*, 9256–9260.
Stout, C. D. (1989) *J. Mol. Biol. 205*, 545–555.
Stout, C. D., Ghosh, D., Pattabhi, V., & Robbins, A. H. (1980) *J. Biol. Chem. 255*, 1797–1800.
Stout, G. H., Turley, S., Sieker, L. C., & Jensen, L. H. (1988) *Proc. Natl. Acad. Sci. U.S.A. 85*, 1020–1022.
Sweeney, W. V., & Rabinowitz, J. C. (1980) *Annu. Rev. Biochem. 49*, 139–161.
Sweeney, W. V., & Rabinowitz, J. C., & Yoch, D. C. (1975) *J. Biol. Chem. 250*, 7842–7847.
Thomson, A. J., & Johnson, M. K. (1980) *Biochem. J. 191*, 411–420.
Thomson, A. J., Robinson, A. E., Johnson, M. K., Cammack, R., Rao, K. K., & Hall, D. O. (1981a) *Biochim. Biophys. Acta 637*, 423–432.
Thomson, A. J., Robinson, A. E., Johnson, M. K., Moura, J. J. G., Moura, I., Xavier, A. V., & LeGall, J. (1981b) *Biochim. Biophys. Acta 670*, 93–100.
Williams-Smith, D. L., Bray, R. C., Barber, M. J., Tsopanakis, A. D., & Vincent, S. P. (1977) *Biochem. J. 167*, 593–600.
Yoch, D. C., & Arnon, D. I. (1972) *J. Biol. Chem. 247*, 4514–4520.
Yoch, D. C., & Carithers, R. P. (1978) *J. Bacteriol. 136*, 822–824.
Yoch, D. C., Benemann, J. R., Valentine, R. C., & Arnon, D. I. (1969) *Proc. Natl. Acad. Sci. U.S.A. 64*, 1404–1410.